Supplementary Materials

Sample Preparation

AuFON

We oxygen plasma cleaned glass coverslips (25 mm diameter, #2) to improve surface hydrophilicity and remove surface contaminants, rinsing the glass coverslips thoroughly with ethanol and deionized water both before and after the plasma etching. We washed a solution of 800 nm diameter silica microspheres (NanoCym, 5% by volume) in Millipore ultrapure water (18 MΩ) and re-diluted to a 5% by volume. We then manually dispersed 25 μL of this solution across the surface of the glass coverslip. We allowed the silica microsphere solution to evaporate under ambient conditions, forming a close-packed monolayer. (*24*) We then deposited $\sim$200 nm of gold on the silica-coated substrates using a thermal evaporation system at a rate of 2 Å/s, with samples rotated at 16 RPM. (CHA Industries, SEC-600). An image of the AuFON substrates is shown in Figure S1A. We prepared a 1 mM solution of methyl viologen dichloride hydrate (Sigma Aldrich, 98%, 75365-73-0) in ethanol (Decon, 95%) and deposited 40 μL on the AuFON for ultrafast SERS measurements.

We measured the localized surface plasmon resonance (LSPR) extinction spectrum of the AuFON with a Shimadzu UV-2600 equipped with an integrating sphere attachment (Shimadzu, ISR-2600). The data acquisition time for each collection was 4 milliseconds. A representative example substrate and extinction spectrum are shown in S1. We collected extinction spectra for all experimental samples before analyte addition, after analyte addition, and after ultrafast experiments.

AuFON Electrode

We prepared the AuFON working electrode pictured in Figure 1C as follows. We cut prepared AuFON substrates into $\sim$ 5 x 10 mm pieces. We then adhered these pieces to a similar sized

piece of 1 mm thick glass slide (Fisherbrand, 12-549-3) with two part epoxy (Locktite Quick Set Epoxy, HC01-81501) and allowed it to cure for 1 hour. We flattened the end of a piece of 14 gauge copper wire and adhered it to one side of the exposed AuFON surface with two part epoxy and allowed to cure for an additional hour. We verified continuity between the copper wire and AuFON surface using a multimeter and encapsulated the remaining exposed copper wire with two part epoxy, allowing the electrode to cure fully in a vacuum desiccator overnight before using in SEC-SERS experiments.

Spectroelectrochemical SERS Instrumentation

For spectroelectrochemical measurements, we used a simple electrochemical cell coupled to a potentiostat (Pine Research, WaveNow Wireless Potentiostat/Galvanostat). We performed all measurements in 0.1 M methyl viologen dichloride in 0.1 M KCl (H_2O) electrolyte solution. The working electrode was a homemade AuFON electrode (S**2**), with a Ag/AgCl reference and gold counter electrode. We obtained cyclic voltammograms of this system at sweep rates from 50 to 1000 mV/s. We stepped the potential in increments of 25 mV from 0-1200 mV, resting for 60 s between steps to allow the system to equilibrate. We collected spontaneous SER spectra using the system described above (probe only), with an average power of 25 mW, and 60 s acquisition time.

Ring Deformation Peak Ratio Calibration

In order to translate changes in the ultrafast SERS MV^0 : $MV^{\bullet+}$ ring deformation peak ratio into relative redox population changes and plasmon-generated potentials, we created a set of calibration curves. First, we correlated the potential dependent SEC-SERS MV^0 : $MV^{\bullet+}$ ring deformation peak ratios to the ${E_{r2}}^0$ reduction peak from the AuFON-MV CV. As stated in the main text, we assume that changes in the ${E_{r2}}^0$ reduction peak amplitude between -0.85 and -1.06

V correspond to a change in the MV^0 population, from $\sim$ 0 to 100%. This assumption ensures that our quantified values are, at worst, underestimated. We approximated the ${E_{r2}}^0$ reduction peak as a Gaussian distribution, onto which we mapped the percentages for MV^0 (S2). From here, we were able to correlate the peak ratio to both % MV^0 (S3) and potential (S4). We created the two necessary calibration curves for translating MV^0 : $MV^{\bullet+}$ ring deformation peak ratios into % MV^0 and applied potential by fitting the linear regime of these correlative plots. The equations for these fits are shown on S3 and S4 respectively. Error in the y-axis for S3 corresponds to the propagated uncertainty in the Gaussian fit of the ${E_{r2}}^0$ reduction peak and error in the x-axis for S3 and S4 corresponds to the propagated uncertainty in the SEC-SERS peak fits.

Ultrafast SERS Instrumentation

Detailed descriptions of our ultrafast SERS instrument have been published previously. (*15–18*) Briefly, we used a Yb-doped fiber-based amplified laser source (Clark-MXR Impulse) to produce $<$250 fs pulses centered at $\sim$1040 nm at a 2.04 MHz repetition rate, with an average power of 15 W (S6). We generated the picosecond probe pulse by sending the incident beam through a spectral filter constructed in a retroreflecting geometry, which contains a transmission grating (LightSmyth Technologies LSFSG-1000-3212-94) to disperse the beam and a 100 mm focal length cylindrical lens (Newport CKX100AR.16) to image the beam onto a slit. (*56*) We determined the spectral FWHM of the filtered output to be 17.9 cm^{-1}, as measured from the 1003 cm^{-1} peak of toluene. We used a 100 mm focal length achromatic lens (Edmund Optics 49-374) to focus the pump and probe beams onto the sample to radii of approximately 180 μm and 160 μm, respectively. The probe power was 10 mW and the pump power ranged from 5 to 11 mW. After the sample, we blocked the pump transmission with a spatial filter, and collimated the spontaneous SERS signal with a 60 mm focal length lens (Thorlabs, LA1134-C). We used

a 100 mm focal length achromatic lens (Thorlabs, AC254-100-C) to focus the SERS signal into a 0.3 m spectrograph (Princeton Instruments SP2300i) equipped with a 300 gr/mm, 1 μm blaze grating. We placed a 1064 nm Raman filter (Edmund Optics 47-510) directly before the spectrograph to remove any remaining $\sim$1040 nm light from the SERS signal. We used a 1024 pixel, liquid nitrogen cooled InGaAs photodiode array (Princeton Instruments PyLoN-IR 1.7) for detection of the Stokes-shifted SER scattering, with an integration time of 20 s for each ultrafast SER spectrum. A schematic depiction of the described setup is shown in S5.

Data Collection and Analysis

Data Collection and Pre-Processing

As described in the main text, we acquired 10 data sets at each incident average pump power, ranging from 5 - 11 mW across 4 substrates. We set the average probe power to $\sim$10 mW (flux, 13.6 W/cm^2) for all experiments. We calculated the pump flux (4.87 - 10.6 W/cm^2) using the measured pump beam diameters listed in the previous section. Here, we outline the general data analysis process used in this work. All analysis was done in IGOR Pro (v7.0.8.1), unless otherwise stated.

For ultrafast measurements, we used a mechanical delay stage (Newport XMS50) in the pump line to control the temporal offset of the pump and probe. We controlled spectral acquisition using a custom Labview code, which automatically randomizes predetermined stage positions (time points) collected for each experiment. We collected three spectra at each timepoint: pump off– or, ground state (GS), -50 ps offset (n50), and the predetermined time offset, or excited state (ES). Commonly, our acquired spectra exhibit high frequency etaloning, which we remove by applying a Fourier filter. We then scaled each spectrum by the incident probe power and acquisition time. We performed an optical Kerr effect measurement

in a 2 mm path-length cuvette of toluene to determine our pump and probe cross-correlation. From this measurement, we calculate the time resolution to be 1.9 ps – the FWHM of the cross-correlation (S7). We note that, on the AuFON, the SERS background differs substantially between the pump-off (GS) and pump-on (n50 and ES) spectra due to scattering from the pump pulse off of the rough and reflective surface. In order to account for the difference in pump-induced SERS background, we describe the ground state in our analysis herein as the n50 spectrum.

Data Analysis

In some cases, the 5 minute wait time prior to running experiments was not long enough to allow for full equilibration of the AuFON-MV system, resulting in spectral anomalies at early acquisition times. To account for this issue, we removed the first three acquisitions for all experiments. Because the time points are randomized and many replicates were taken, there was still ample data for analysis at each time point. Using a custom macro, we fit the 1030 cm^{-1} and 1070 cm^{-1} ring deformation modes of MV^0 and $MV^{\bullet+}$ as a pair of Gaussian peaks for every pre-processed ES and corresponding n50 spectrum (S8, A/B).We calculated the peak ratio for the ES and n50 individually from the fit amplitudes, and calculated the change in peak ratio (Δ_{n50} peak ratio) as *peak ratio*$_{ES}$ - *peak ratio*$_{n50}$. For the kinetic representation in figure 3A, we fit the full set of time-dependent mean Δ_{n50} peak ratios for each pump power to a convolution of the Gaussian instrument response and single exponential decay using the Global Fit module in IGOR Pro. For quantification of Δ % MV^0 and Δ potential, we fit each individual data set with the same fit function, as shown in S8, C. Error bars here represent the propagated peak amplitude fit error for the MV^0 : $MV^{\bullet+}$ peak ratio. We took the amplitude of the Gaussian component of these fits as the maximum Δ_{n50} peak ratio (grey dots, S9). Outliers from each

pump power data set were detected with a generalized extreme studentized deviate (ESD) test from the PyAstronomy package in Python 3. We subsequently removed these outliers from each data set. We then performed a one-sided ANOVA analysis to determine significance of the linear trend of Δ_{n50} peak ratio with pump flux (Table 1; F=8.21, P=0.00034), and a Tukey (HSD) test to analyze the significance of the offset between individual sets (Table 2). Next, we averaged the peak ratios for all 10 experiments at each pump power to calculate a set of mean Δ_{n50} peak ratios, with error propagated from the ultrafast/SEC-SERS peak fits (y-axis) and the measured pump powers/beam area (x-axis) (blue dots, S9). Subsequently, we used these mean values to calculate the $\Delta\%\mathrm{MV}^0$ and potential in Figure 3 using the linear fit equations in S3 and S4.

For analysis of the long-lived reduced MV^0 population, we averaged the mean of the Δ_{n50} peak ratios for the 30, 40, and 50 ps time points for each data set. We calculated the average of this mean value for all experiments at each pump power to give the average mean Δ_{n50} peak ratio for t=30-50 ps, with error propagated from the ultrafast/SEC-SERS peak fits (y-axis) and the measured pump powers/beam diameters (x-axis) (S10). We performed a one-sided ANOVA analysis to determine if the linear relationship between the average mean Δ_{n50} peak ratio (t=30-50 ps) and pump flux was statistically significant (Table 3; F=2.81, P=0.058) – although not significant, there is a perceivable positive trend between the sets. We then performed individual T-tests on each set to analyze the significance of their offset from zero (Table 4). Similarly as described above, we converted these peak ratios to $\Delta\%\mathrm{MV}^0$ and potential using the linear fit equations in S3 and S4.

Ground State Addition Spectra for Visualization of Transient Features

In order to prepare a qualitative visualization of the transient changes to the MV^0 : $\mathrm{MV}^{\bullet+}$ ring deformation peak ratio in our ultrafast SERS experiments, we display transient spectra

shown in Figure 2 of the main text in a form that is referred to as ground state addition spectra (GSA). For each time point, we performed a 1:1 subtraction of the ES and n50, creating a depletion spectrum. Using a custom fitting macro, we first fit a characteristic depletion feature to a negative Gaussian line shape. Using the amplitude of that fit, we calculated a percentage of the n50 to add back to the depletion spectrum so that the amplitude at that specific peak frequency would be equal to zero. The new spectrum created in this process is called a GSA spectrum. Doing this at every time point emphasizes positive changes in the transient ultrafast SERS spectra, as shown in Figure 2 of the main text. This preparation is only used to visualize small transient changes in SERS spectra, and is not used for further quantification.

Fitting MV^0 Excited Vibrational State Feature

In order to approximate the time dependent behavior of the feature red-shifted from the 1030 cm^{-1} MV^0 ring deformation peak, we fit the shoulder and 1030 cm^{-1} peak to a pair of Gaussian distributions for the n50 and ES data sets for one experiment in the 10.6 W/cm^2 pump power series. The frequency of the shoulder feature was held at 1017 cm^{-1}, in accordance with our anharmonic DFT frequency analysis (Table 5). We calculated the 1017 cm^{-1} and 1030 cm^{-1} peak areas from the fits. We then calculated the percent contribution of the 1017 cm^{-1} peak to the total area of both peaks for both the ES and n50. Finally, we took the difference of the percent contribution of the 1017 cm^{-1} peak for the ES and n50 spectra, giving the plot shown in S12. Here, we see an approximate change in contribution for the 1017 cm^{-1} peak at time zero of 3%.

From the same data set, we calculated an approximate increase in MV^0 of 3% from the 1030:1070 cm^{-1} peak ratio using methods described above. Using this value, we can extrapolate that there is an additional 0.1% increase in the MV^0 population owed to MV^0 molecules in excited vibrational states.

DFT Calculations of MV

In order to confirm the vibrational assignments of the Raman modes observed in the ultrafast and SEC SERS experiments, we referenced literature values (*34, 35*) and performed DFT-based optimization and vibrational frequency calculations for MV^0, $MV^{\bullet+}$,and MV^{2+} with Gaussian 16 using the B3LYP functional and 6-31G** basis set. In these calculations, we included a Self-Consistent Reaction Field (SCRF) using the default Polarizable Continuum Model and integral equation formalism variant. We attempted to make calculations including the gold surface using higher-level models, but the results significantly deviated from experimental observations. The level of theory used here is acceptable for calculations of radical species, (*57–59*) and the calculated frequencies match closely to experimental observations. From our calculations, we can assign the 990/1020 cm^{-1} (SEC-SERS) and 1030/1070 cm^{-1} (ultrafast SERS) peak pairs to a C-N stretch/in-plane ring deformation motion. Figure S11 shows the scaled (0.961) calculated spectra for MV^0 (yellow), $MV^{\bullet+}$ (red),and MV^{2+} (blue), with peaks for the calculated frequencies broadened to 18 cm^{-1} to match our experimental parameters. Anharmonic frequency calculations were performed using the same functional and basis set, with omission of the SCRF.

MV Surface Concentration Estimation

We were able to estimate the number of MV molecules deposited onto the AuFON surface to an upper limit using a molecular packing density of 1 x 10^{-10} mol cm^2 for pyridine. Assuming MV is adsorbed parallel to the AuFON surface and has an area comparable to two adjacent pyridines, this is a reasonable order of magnitude estimation. (*52*) In order to account for the nanostructure of the AuFON, we used a geometric model to calculate a scaling factor of 2.6 for

the probed area (F_{sc}) – assuming a monolayer of half prolate ellipsoids.

$$F_{sc} = \frac{\pi\sqrt{3}(2r+h)}{6\sqrt{1-\frac{r^2}{(r+h)^2}}} \sin^{-1}\sqrt{1-\frac{r^2}{(r+h)^2}} \tag{1}$$

Here, r is the radius of the silica nanospheres (400 nm) and h is the thickness of the gold layer (200 nm). Using this, we estimate the number of MV molecules within the probed region to be $\sim$ 2 x 10^{11}. Assuming half of the starting molecules are $MV^{\bullet+}$, then for the reduction of $MV^{\bullet+}$ to MV^0, we observe a transient conversion on the order 10^9 of molecules at time zero in the ultrafast SERS experiments, and a conversion of approximately one molecule per pulse for the MV^{2+} to $MV^{\bullet+}$ reduction in the steady state. If we have $\sim$ 3 x 10^{16} photons per pump pulse (10.6 W/cm^2 pump flux), this translates to a quantum yield for reduced species on the order of 10^{-5} % and 10^{-14} % respectively.

References

24. L. A. Dick, A. D. McFarland, C. L. Haynes, R. P. Van Duyne, Metal film over nanosphere (MFON) electrodes for surface-enhanced Raman spectroscopy (SERS): Improvements in surface nanostructure stability and suppression of irreversible loss, *Journal of Physical Chemistry B* **106**, 853–860 (2002).

15. E. L. Keller, R. R. Frontiera, Monitoring Charge Density Delocalization upon Plasmon Excitation with Ultrafast Surface-Enhanced Raman Spectroscopy, *ACS Photonics* **4**, 1033–1039 (2017).

16. E. L. Keller, R. R. Frontiera, Ultrafast Nanoscale Raman Thermometry Proves Heating Is Not a Primary Mechanism for Plasmon-Driven Photocatalysis, *ACS Nano* **12**, 5848–5855 (2018).

17. N. C. Brandt, E. L. Keller, R. R. Frontiera, Ultrafast Surface-Enhanced Raman Probing of the Role of Hot Electrons in Plasmon-Driven Chemistry, *Journal of Physical Chemistry Letters* **7**, 3178–3185 (2016).

18. Z. Yu, R. R. Frontiera, Intermolecular Forces Dictate Vibrational Energy Transfer in Plasmonic-Molecule Systems, *ACS Nano* **16**, 847–854 (2022).

56. S. Shim, R. A. Mathies, Generation of narrow-bandwidth picosecond visible pulses from broadband femtosecond pulses for femtosecond stimulated Raman, *Applied Physics Letters* **89**, 121–124 (2006).

35. S. Ghoshal, T. Lu, Q. Feng, T. M. Cotton, A normal coordinate analysis of the vibrational modes of the three redox forms of methylviologen: Comparison with experimental results, *Spectrochimica Acta Part A: Molecular Spectroscopy* **44**, 651–660 (1988).

220 34. A. di Matteo, Structural, electronic and magnetic properties of methylviologen in its re-
221 duced forms, *Chemical Physics Letters* **439**, 190–198 (2007).

222 57. L. Yu, *et al.*, Substituent effects on radical cations of halogenated biphenyl compounds: A
223 density functional theory and time-resolved resonance Raman study, *Research on Chemical*
224 *Intermediates* **27**, 485–501 (2001).

225 58. J. T. Godbout, *et al.*, Resonance Raman studies of phenylcyclopropane radical cations,
226 *Journal of Raman Spectroscopy* **31**, 233–241 (2000).

227 59. J. Szczepanski, *et al.*, Vibrational and electronic spectroscopy of the fluorene cation, *Jour-*
228 *nal of Physical Chemistry A* **106**, 63–73 (2002).

229 52. L. Stolberg, S. Morin, J. Lipkowski, D. E. Irish, Adsorption of pyridine at the Au(111)-
230 solution interface, *Journal of Electroanalytical Chemistry* **307**, 241–262 (1991).

SI Figures

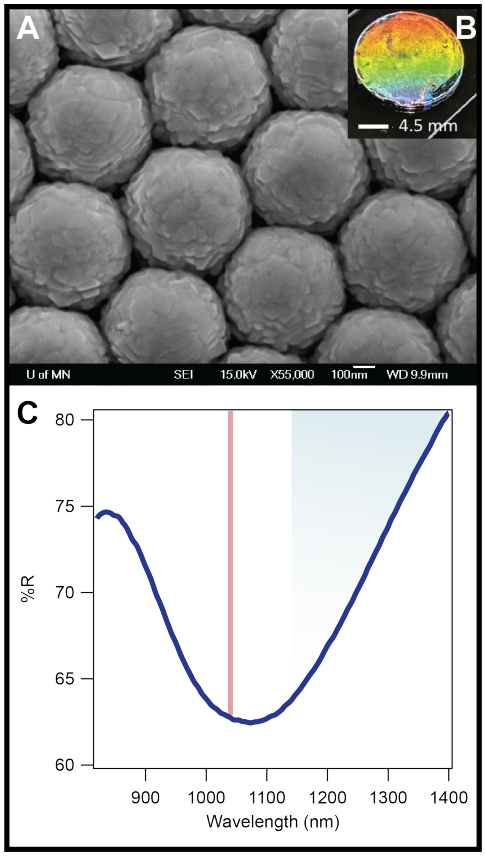

Figure S1: A) SEM Image of AuFON substrate. B) Full-scale image of AuFON substrate. C) Reflection spectrum of AuFON used in these experiments, with maximum extinction given as the minima of the reflectance spectrum at 1075 nm. The red line shows our excitation wavelength at $\sim$1040 nm, and the green shaded region shows the region of interest for detecting SER scattered photons.

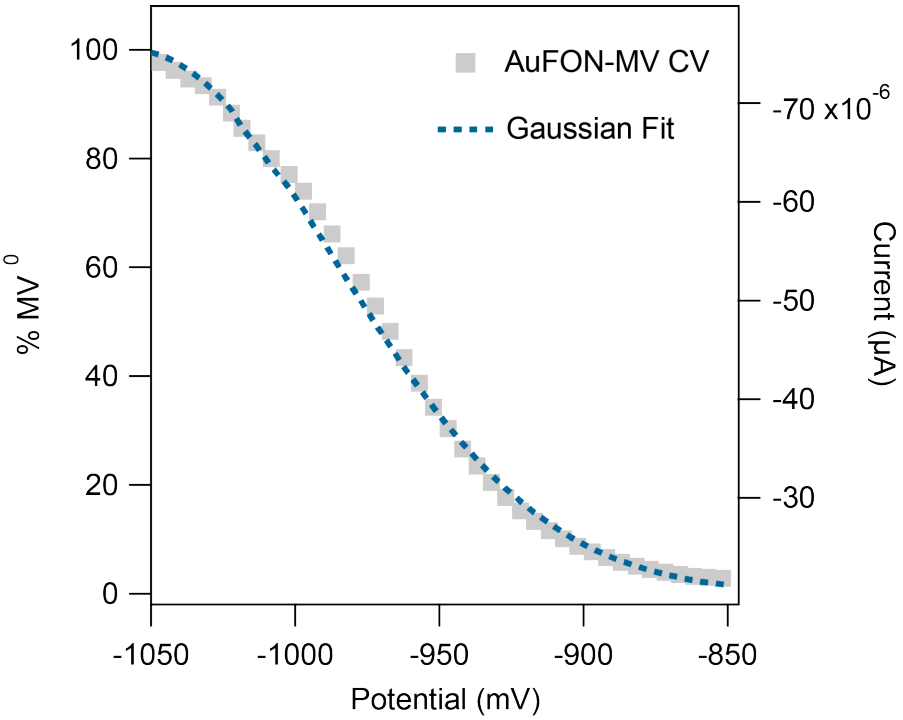

Figure S2: Correlation of [MV^0] with potential.

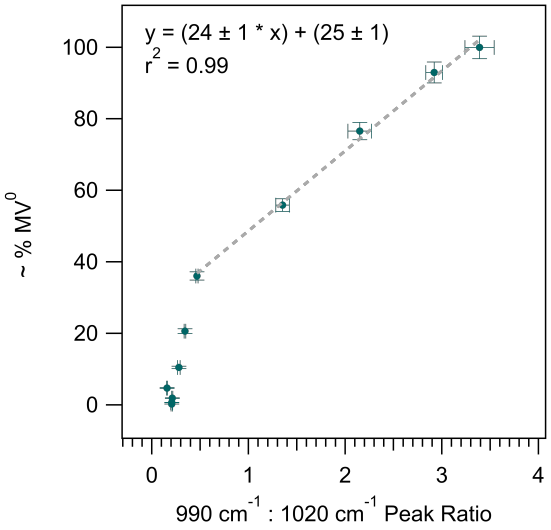

Figure S3: Calibration curve, translating SEC-SERS ring deformation peak ratio to % MV^0

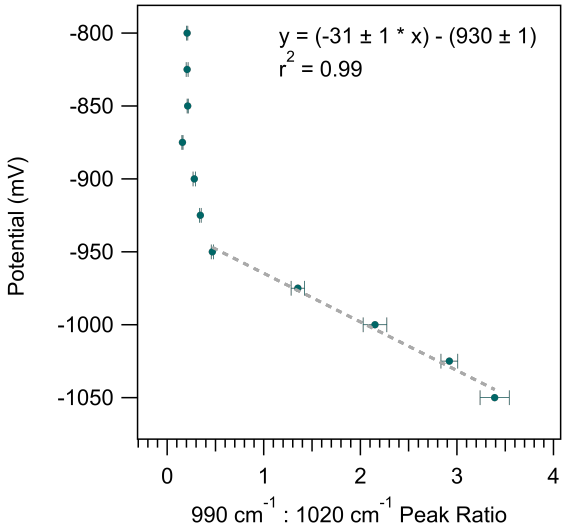

Figure S4: Calibration curve, translating SEC-SERS ring deformation peak ratio to potential

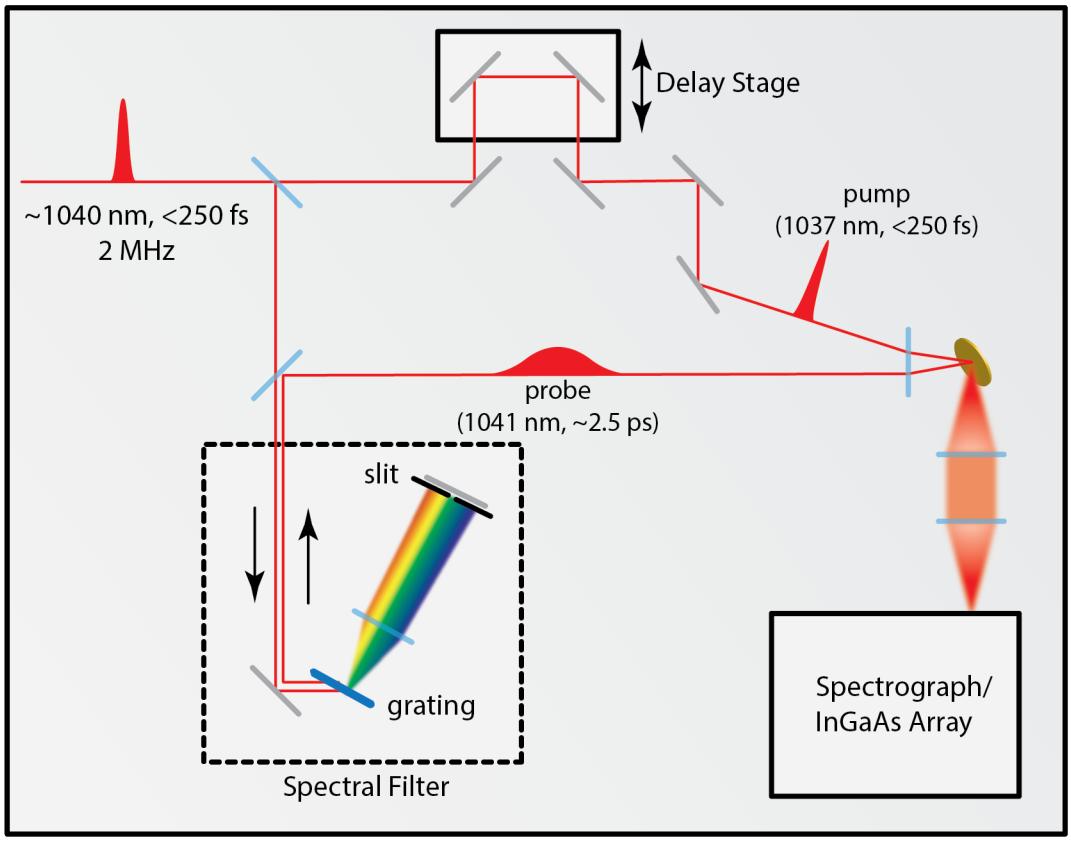

Figure S5: Schematic depiction of ultrafast SERS experimental setup.

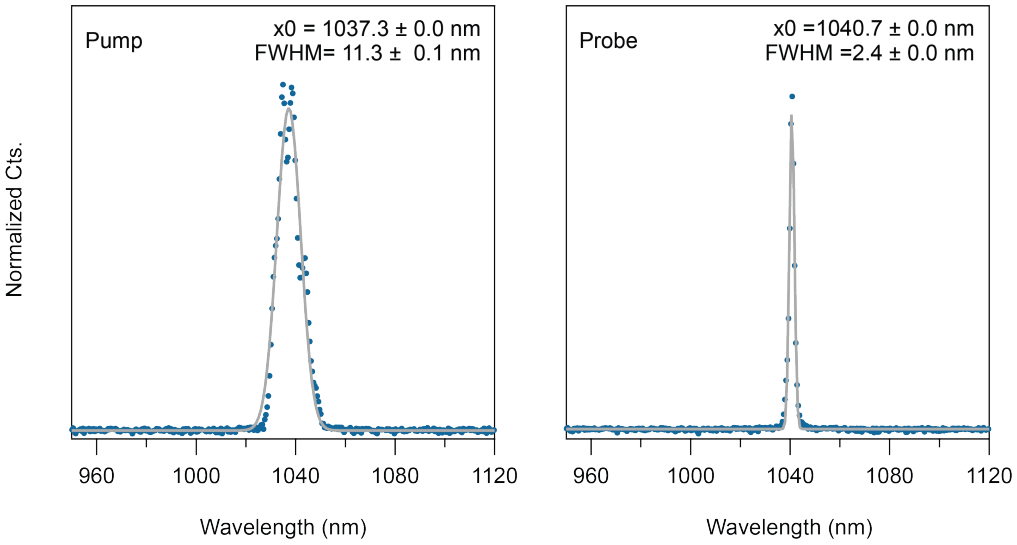

Figure S6: Spectra of pump and probe used in ultrafast SERS and SEC-SERS measurements. The pump is centered at 1037 nm, and the probe at 1041 nm.

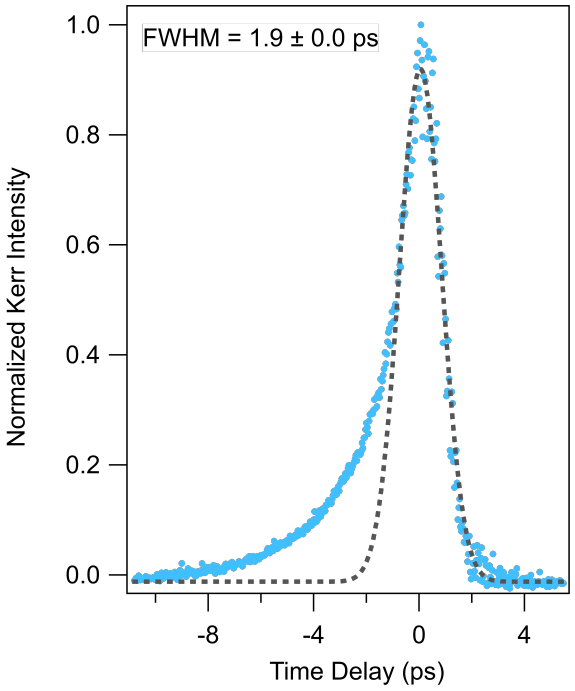

Figure S7: Representative pump/probe cross-correlation measurement using the optical Kerr effect. The peak is fit to a Gaussian lineshape, with a FWHM of 1.9 ps. The tail at negative timepoints is due to spatial chirp of the pump beam.

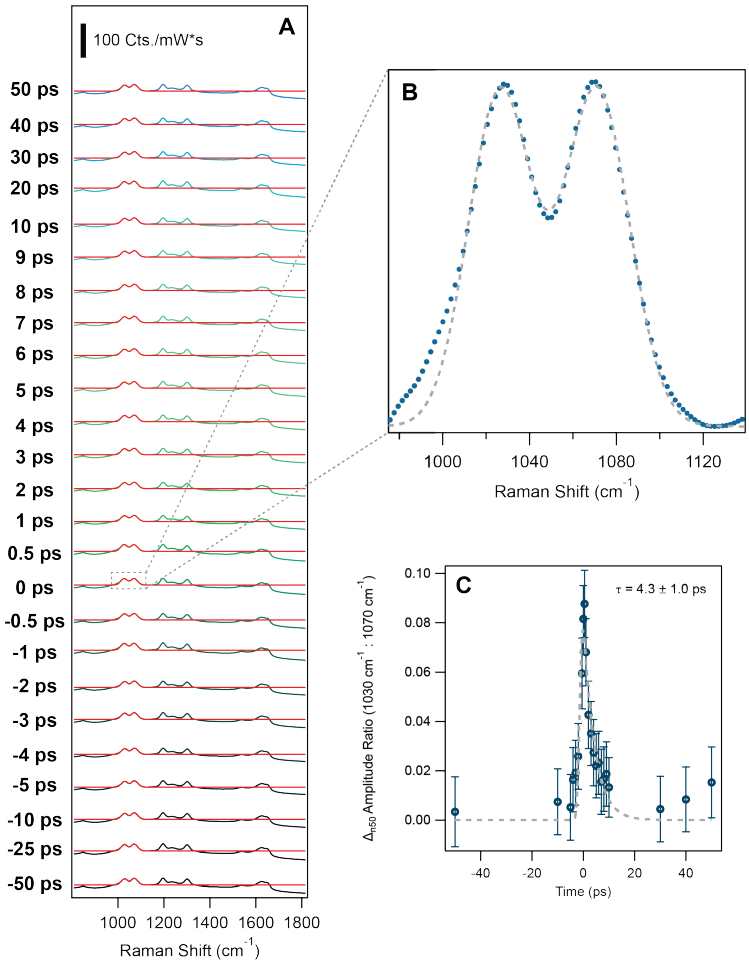

Figure S8: Examples from workup of one data set at 10.6 W/cm^2 pump flux. A) Individual fits of 1030 cm^{-1} and 1070 cm^{-1} peaks from ES spectra. B) Detailed image of fit for 0 ps spectrum. C) Resulting kinetic trace for this data set after subtracting fits from n50 spectra.

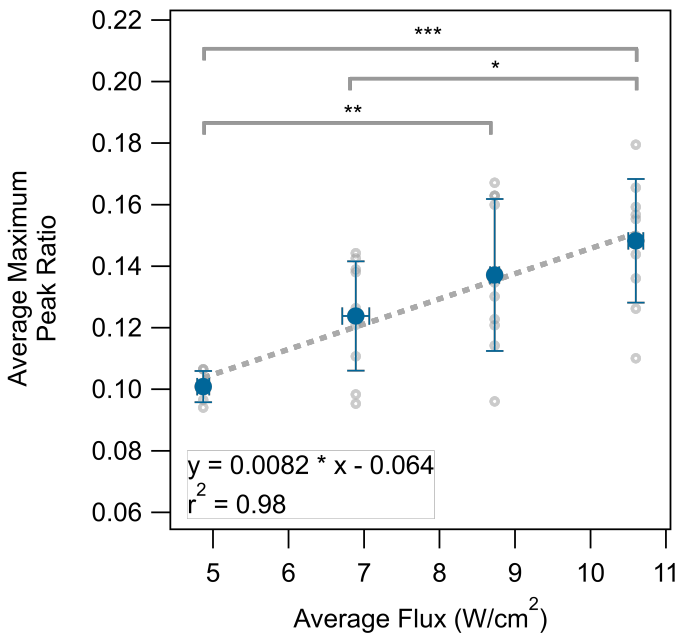

Figure S9: Maximum peak ratio at each pump power. Grey markers indicate individual experiments and blue markers represent the average of those experiments. The linear trend of the average peak ratio is significant (ANOVA [F=8.21, P=0.00034]). Significance of offset between individual experiments is given by the asterisks (* = P$\leq$ 0.05, ** = P$\leq$ 0.01, and *** = P$\leq$ 0.001).

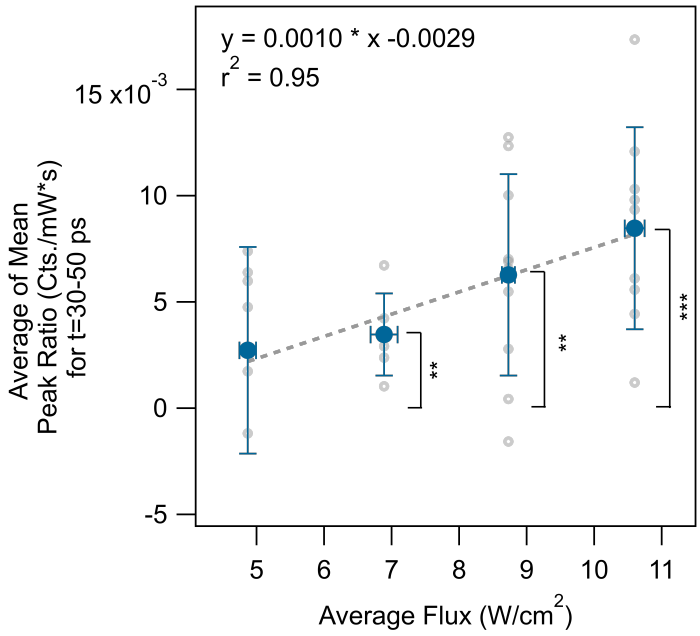

Figure S10: Mean of peak ratio for t=30 - 50 ps at each experimental pump power. Grey markers indicate individual experiments and blue markers represent the average of those experiments. The linear trend of the peak ratio is not significant, but there is a clear positive trend (ANOVA [F=2.81, P=0.058]). Significance of offset between individual experiments is given by the asterisks (* = P$\leq$ 0.05, ** = P$\leq$ 0.01, and *** = P$\leq$ 0.001).

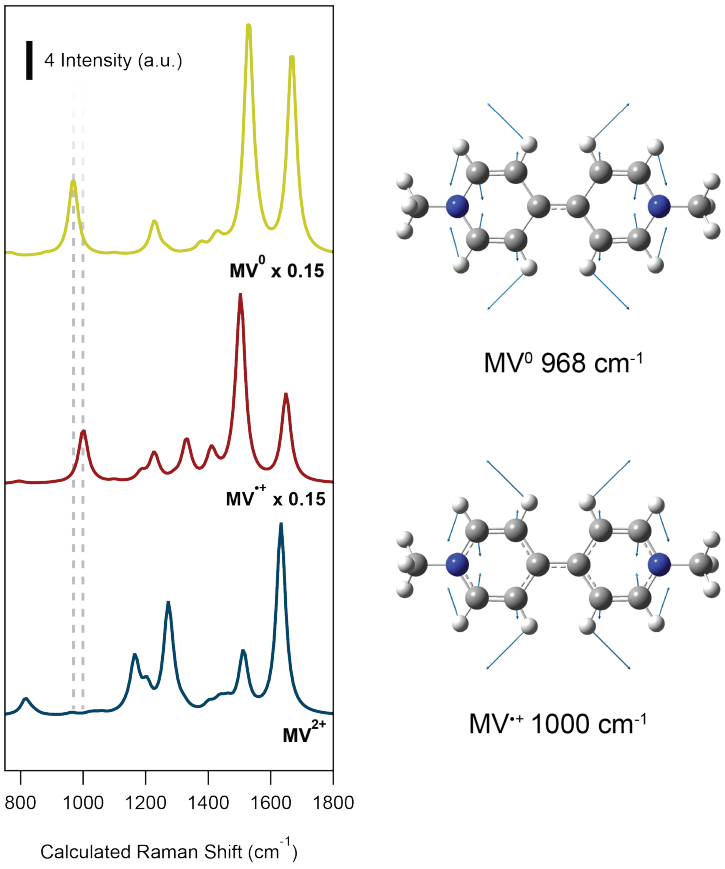

Figure S11: DFT calculated Raman spectra for MV^0, $MV^{\bullet+}$,and MV^{2+}, showing the same ring deformation modes observed in our SERS experimenst at 968 cm^{-1} and 1000 cm^{-1}. The displacement vectors for the at 968 cm^{-1} (MV^0) and 1000 cm^{-1} ($MV^{\bullet+}$) modes are displayed, confirming that this is the same mode in both redox states.

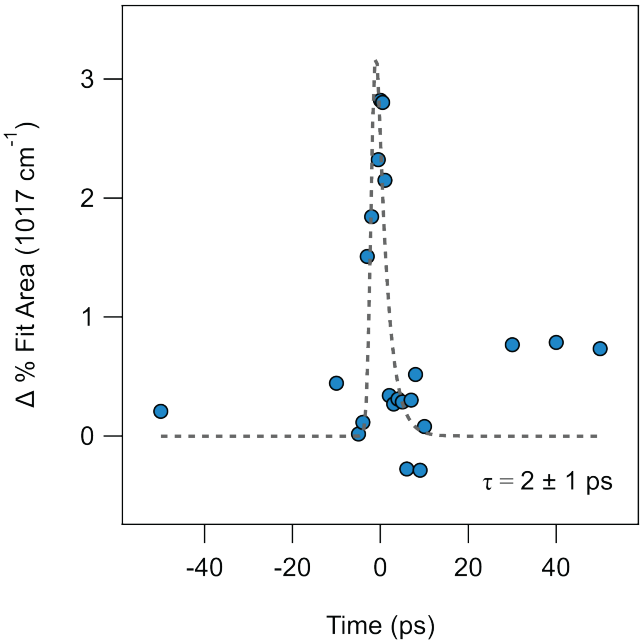

Figure S12: Typical kinetic trace showing the change in percent fit area for the 1017 cm^{-1} shoulder component of the 1032 cm^{-1} and 1017 cm^{-1} peak pair at 10.6 W/cm^2 pump power.

SI Tables

	DF	SS	MS	F	Fc	P
Groups	3	0.000931	0.00310			
Error	32	0.0121	0.000378			
Total	35	0.0214	0.000612	8.21	2.90	0.000341

Table 1: ANOVA analysis of data sets in Figure S9.

Comparison (W/cm2)	Difference	SE	q	q0.05_32_4	Conclusion	P
10.6 -- 4.87	0.0474	0.00710	6.68	3.83	Significant	0.000251
10.6 -- 6.89	0.0244	0.00615	3.97	3.83	Significant	0.0400
10.6 -- 8.73	0.0111	0.00615	1.80	3.83	Not Significant	0.585
8.73 -- 4.87	0.0363	0.00710	5.11	3.83	Significant	0.00533
8.73 -- 6.89	0.0133	0.00615	2.17	3.83	Not Significant	0.430
6.89 -- 4.87	0.0230	0.00710	3.23	3.83	Not Significant	0.122

Table 2: Tukey (HSD) Test comparing data sets in Figure S9.

	DF	SS	MS	F	Fc	P
Groups	3	0.000163	5.45E-05			
Error	28	0.000543	1.94E-05			
Total	31	0.000707	2.28E-05	2.81	2.95	0.058

Table 3: ANOVA analysis of data sets in Figure S10.

flux (W/cm^2)	n	DF	avg	stdev	sxBar	t statistic	critical	P	Conclusion
4.87	10	6	0.00272	0.00486	0.00184	1.48	2.45	0.189	Not Significant
6.89	10	5	0.00346	0.00193	0.000787	4.40	2.57	0.00702	Significant
8.73	10	9	0.00627	0.00474	0.00150	4.18	2.26	0.00236	Significant
10.6	10	8	0.00846	0.00475	0.00158	5.34	2.31	0.000692	Significant

Table 4: TTests comparing offset from zero for data sets in Figure S10.

ω (cm^{-1})	993.66
$\Delta\omega$ (cm^{-1})	-16.99
I (km/mol)	0.0005
ΔI (km/mol)	0.0005

Table 5: Output of the anharmonic vibrational analysis of the MV^0 ring deformation mode.